Chapter 1

Experimental and Theoretical Studies on the Dynamics of Transient Plasmas Generated by Laser Ablation in Various Temporal Regimes

Petru-Edward Nica, Stefan Andrei Irimiciuc, Maricel Agop, Silviu Gurlui, Michael Ziskind and Cristian Focsa

Additional information is available at the end of the chapter

http://dx.doi.org/10.5772/intechopen.70759

Abstract

During the last decade, our groups have performed systematic experimental studies on the characterization of plasma plumes generated by laser ablation in various temporal regimes (ns, ps, fs) on materials ranging from simple metals (Al, Cu, Mn, Ni, In, W, …) to more complex compounds (ceramics, chalcogenide glasses, ferrites). Optical (fast imaging and space- and time-resolved emission spectroscopy) and electrical (mainly Langmuir probe) methods have been applied to experimentally investigate the dynamics of the plasma plume and its constituents. Influence of the target physical (thermodynamic and electrical) parameters on the plasma dynamics has been studied. A mathematical correlation between the local and global plasma parameters and the physical properties of the target was proposed for the first time. Peculiar behaviors like plume splitting or plasma oscillations have been evidenced for high laser fluence ablation in vacuum. Along with results from the literature, our findings provide convincing arguments for the existence of multiple double-layers in the laser ablation plasma plume, in a scenario including two-temperature electrons. New fractal-based theoretical approaches have been developed to qualitatively and quantitatively account for the observed phenomena. The space and time evolution of expansion velocity, particle number, current density and plasma temperature were theoretically investigated.

Keywords: laser ablation, transient plasma dynamics, plasma oscillations, Langmuir probe, optical emission spectroscopy, plasma simulation, fractal, hydrodynamics

1. Introduction

Despite its widespread use in a large number of applications (e.g. pulsed laser deposition [1], generation of nanoparticles [2, 3], chemical analysis [4, 5] or cleaning of delicate artwork [6]), a comprehensive picture of laser ablation remains a challenge for both experimentalists and theoreticians. The difficulty arises from the multi-physics nature of the ablation process, coupling optics and electrodynamics (absorption of light by the target material), thermodynamics (heating, phase transitions, cooling), gas dynamics (expansion of ablation plume into vacuum or background gas), plasma physics (collisions, electric interactions) and laser-plume interaction (plasma heating by absorption of laser photons, inverse Bremsstrahlung, multi-photon ionization), some of these evolving on very short time scales, which can make it challenging to find the adequate resolving probe. Moreover, the fundamental mechanisms involved in the ablation process and the properties and dynamics of the subsequent laser-produced plasmas depend strongly on the laser beam parameters (pulse duration, fluence, wavelength or beam profile) and also on the properties of the irradiated material (thermal/electrical conductivity, reflectivity, heat of vaporization, binding energy, etc.).

Fundamental differences can be revealed when investigating the role of the laser pulse duration with respect to the specific timescales of the irradiated material response [7]. For instance, in nanosecond ablation regime, the laser pulse is significantly longer than the usual electron cooling time (∼10 fs) and the lattice heating time (∼ps). In this case, the energy absorbed by the electrons has enough time to be transferred to the lattice. The electrons and the lattice can further reach thermal equilibrium, and the main energy loss is the heat conduction into the solid target. Consequently, the mechanisms involved in this ablation regime are mainly thermal (e.g. phase explosion, normal vaporization, etc.) [8, 9]. Most notably, the subsequent plasma generated in this ablation regime absorbs a significant percentage of the beam energy (pulse "tail", during several nanoseconds), leading to an important heating of the plume. In the case of ultra-fast laser ablation (∼fs), when the laser pulse duration is shorter than (or on the same scale as) the electron cooling time, the electrons in the surface layer suffer cooling by heat diffusion and by heat transfer to the lattice ions. This stage continues for several picoseconds. The picture changes in the case of a semiconductor target which is heated by an ultrashort pulse. In the latter case, laser energy is transferred into the solid by creating a "bath" of hot electrons and holes [10]. Hot carriers subsequently transfer energy to the lattice by creating optical and acoustic phonons. In the case of both metals and semiconductors, the thermalization of laser energy in the hot carrier bath takes place within a few femtoseconds, while the typical time-scale for lattice heating falls within the 1–10 ps range, where thermal conduction is negligible [11]. For low fluence fs-laser irradiation, the Coulomb explosion [12] is the dominant ejection mechanism, while at sufficiently high laser intensities the phase explosion is followed by non-thermal vaporization of the bulk material and becomes the main mechanism for material removal [13]. A particular case of ultra-fast laser ablation is represented by ps-laser ablation. This temporal regime acts like a bridge between the previous cases manifesting characteristics from both regimes. The pulse duration is long enough so that some thermal damage occurs due to the heating of the lattice. If the laser pulse width is in the 1–10 ps range, the particle ejection is still dominated by the Coulomb explosion with minimal contribution

from the thermal mechanism and no interaction between the plasma plume and the incoming laser beam. For longer pulse durations (~100 ps) the balance is "tipped" in favor of thermal mechanisms coupled with a brief absorption of the laser beam by the ejected cloud [7].

Extensive efforts have been fostered by many research groups in the last decades for unveiling this complexity. Most of them were dedicated to characterizing the laser-produced plasma dynamics and to establishing a link between the local/global plasma parameters and the fundamental ablation mechanisms, some also addressed the link with the physical properties of the irradiated material (see, e.g., [14–48]). In order to draw a comprehensive picture of the laser-produced transient plasma evolution, one needs detailed space- and time-resolved information on the chemical and electrical composition of the expanding plume (ions, electrons, neutral atoms, molecules, clusters, with associated number densities, ionization stages, etc.), the plasma dynamics—expansion regime (plasma as a whole), kinetic energies (of every individual species), etc. Optical (fast photography, shadowgraphy, interferometry, optical emission and absorption spectroscopies, laser-induced fluorescence, resonant ionization spectroscopy, Thomson scattering) and electrical (Langmuir probes (LP), Faraday cups, electrostatic analyzers, mass spectrometry) methods [49, 50] are available for undertaking this complex investigation. The difficulty in getting a complete description of the laser ablation plasma plume arises mostly from its transient character, with a lifetime typically on the 10 μs scale, but with inner rapid phenomena (e.g. oscillations) which can exhibit sub-nanosecond timescales. Consequently, extreme care must be taken for the specific application of well-known steady state plasma characterization tools (e.g. Langmuir probes) to this transient case. Moreover, not all of the above-mentioned techniques can be applied for probing the great variety of laser ablation plasmas (nor even one given plasma plume along its spatial and temporal evolution). For instance, higher electron number densities are needed to get an effective response when using interferometry or Thomson scattering than when Langmuir probes are used. Typical irradiation conditions (in the range of GW/cm^2) will result in laser ablation plasmas which can be considered as cold (electron temperature in the eV range, number densities roughly in the 10^{13}–10^{18} cm^{-3} range). Higher irradiation values (exceeding 1 PW/cm^2) can lead to hot plasmas with higher electron temperature and number densities, usually studied in a laser inertial confinement nuclear fusion context [51].

During the last decade, our groups have performed systematic experimental and theoretical studies on the fundamental characterization and applications (mainly pulsed laser deposition of thin films) of plasma plumes generated by laser ablation in various temporal regimes (ns, ps, fs) on materials ranging from simple metals (Al, Cu, Mn, Ni, In, W, etc.) to more complex compounds (ceramics, chalcogenide glasses, ferrites) [52–79]. Optical (fast gate Intensified Charge Coupled Device (ICCD) camera imaging and space- and time-resolved emission spectroscopy) and electrical (mainly Langmuir probe) methods have been applied to experimentally investigate the dynamics of the plasma plume and its constituents. The analysis of probe current-voltage characteristics at various delays after the laser pulse gave access to the temporal evolution of ion density, electron temperature and plasma potential. The recording timescales are analyzed by coupling the distribution functions of electrons and ions through an effective mass. The space and time evolution of expansion velocity, particle current density and plasma temperature were theoretically investigated by a fractal hydrodynamic model. We

present here a short overview of these experimental and theoretical studies, with a special focus on the characterization of transient laser-produced plasmas by electrical methods and on recent developments of the fractal hydrodynamic model.

2. Experimental details

A schematic view of the experimental set-up often used in our studies is given in **Figure 1**. The solid targets (usually 20 mm diameter, 1 mm thick disks) of various chemical composition were placed on a translation-rotation stage in vacuum or controlled atmosphere and irradiated by ns, ps or fs laser pulses at various wavelengths (usually 532 nm Nd:YAG and 800 nm Ti:Sa, Quantel, Continuum, Spectra Physics). We used laser fluences spanning the 10^{-1}–10^{3} J/cm^2 range, corresponding to irradiances in the 10^{6}–10^{14} W/cm^2 limits for laser spot dimensions on the target in the range 0.1–1 mm and laser pulse durations in the range 40 fs–10 ns.

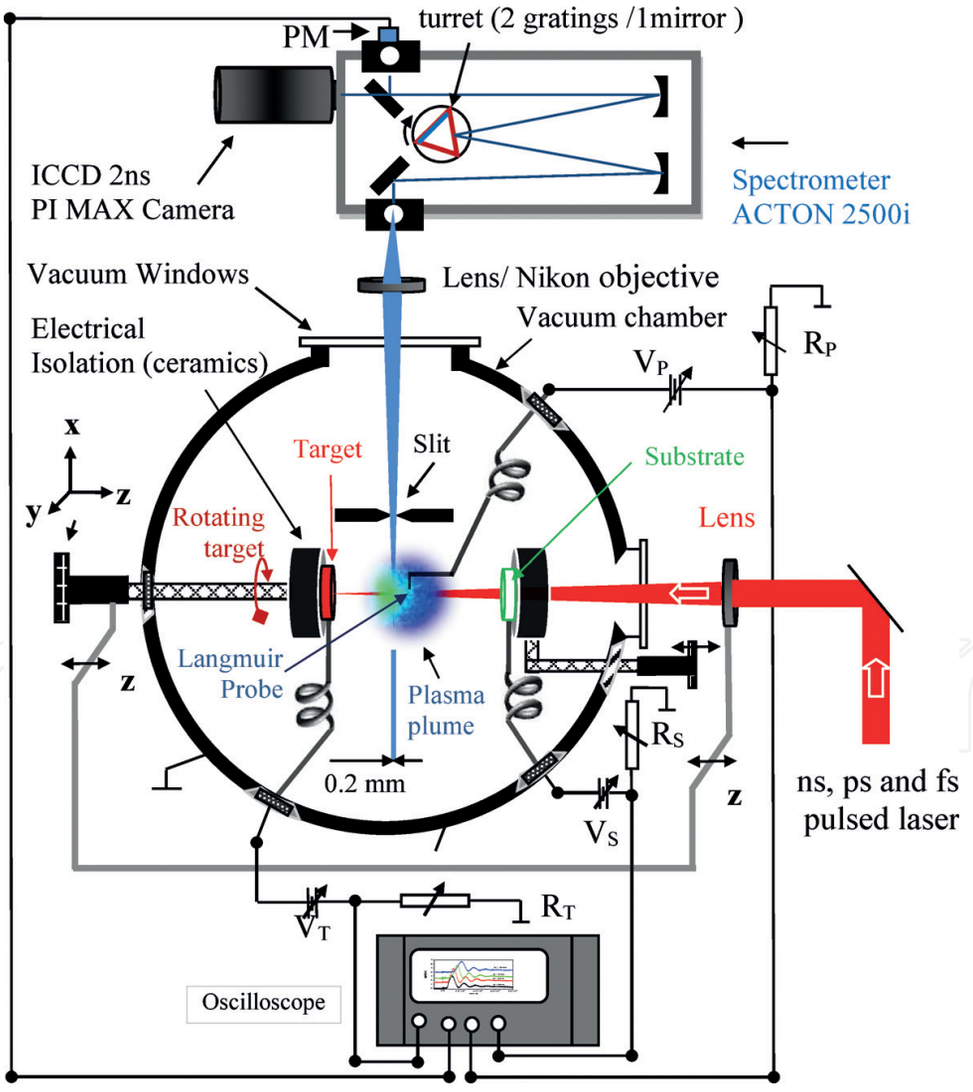

Figure 1. Schematic view of the experimental set-up at the University of Lille.

The electric diagnostics mainly used were Langmuir probes immersed at various positions in the plasma plume to record the ionic or electronic currents, depending on the probe biasing voltage (V_P) [52, 53, 55, 58, 60, 77, 79]. Using bunches of Langmuir probes we obtained the angular distribution of charge carriers at various distances from the target [52]. The Langmuir probes were 0.8 mm diameter, 5 mm length stainless steel wires. When using metallic targets, they were also biased to observe the influence on the probe current, and to correlate it with the transitory electrical signal recorded from the target [65]. The transitory signals were registered by digital oscilloscopes with 0.5–2 GHz bandwidth (LeCroy) using 50 Ω or 1 MΩ impedances.

To record the plasma optical emission, three configurations have been often used: plasma plume imaging (ICCD fast photography), space- and time-resolved optical emission spectroscopy (OES) and temporal evolution of a given spectral line intensity [54–57, 62, 64, 66–68, 73, 75]. For the imaging experiments, ICCD gate widths of 5 ns were usually employed in order to catch as much as possible sharp temporal snapshots in the space-time evolution of the plume. For space-resolved OES, a 1 mm × 5 mm translating slit was placed in the vacuum chamber, at 40 mm from the normal to the target, to observe plasma plume "slices" of 1 mm width [57]. Finally, the temporal evolution of a given spectral line intensity was recorded with a fast (sub-ns rise-time) photomultiplier tube (PMT, Hamamatsu) placed on the second output port of the monochromator (Acton Princeton Instruments), once the spectral line has been selected and isolated with appropriate entrance and exit slit widths and diffraction grating positions [54, 57].

3. Experimental results

Both our optical and electrical investigations on the dynamics of the transient plasmas produced by laser ablation in vacuum revealed some peculiar phenomena as the plume splitting in (at least) two components or the occurrence of oscillations in the currents recorded by the Langmuir probe or on the irradiated target. We have recently presented an overview of these peculiar findings, along with similar results from the literature, in a review paper [78]. We will therefore orient the presentation below more on the extraction of significant plasma parameters (to be compared with the theoretical model predictions) from the time-of-flight profiles of the currents recorded by the LP.

The typical time-evolution of the ion current recorded by the probe placed at various distances (axial, radial) with respect to the center of the laser irradiation spot shows that it extends in the μs range and it generally consists in a fast part having an oscillatory behavior, and a slower tail which arrives at longer times (see some examples in **Figure 2**, for ns-ablation and $V_P = -30$ V probe biasing). As it was expected, the time at which the first current maximum is recorded (t_{max}) significantly increases with the distance from the target (z), while it is only slightly increasing with the radial distance (r). Moreover, for $r > 1$ cm and $z > 3$ cm the oscillations disappear. In a simple estimation, the z-t_{max} dependence, displaying a linear evolution, gives an axial expansion velocity $v_z = 1.25 \times 10^5$ m/s. Also, a decrease of t_{max} when increasing the laser pulse energy was evidenced in our previous work [55], as a consequence of the higher expansion velocity. For comparison, from the time-evolution of the optical maximum signals

recorded by ICCD imaging, one can derive the center-of-mass velocities of the plasma structures [55,56,62]. In all our studies, we found values in the range of 10^4 m/s for the first (fast) structure and of 10^3 m/s for the second (slow) one, in agreement with experimental results given in the literature [80–82] and rough calculations performed in simple thermodynamic framework [58, 59]. As an example, for the experimental conditions in which the data from **Figure 2** were registered [55], we have obtained v_{fast} = 4.66 × 10^4 m/s which is half of the previous value, as consequence of ion acceleration/oscillation in the probe electric field. Moreover, by smoothing the probe signal to remove the oscillations, the temporal trace is well described by a shifted Maxwellian velocity distribution function [83, 84], with center-of-mass (or "drift") velocity in the range of 10^4 m/s [77].

The currents induced in the target by the ablation process (displayed in **Figure 3a** for various laser energies/pulse) can be correlated with the probe signal, as the positive charging arises

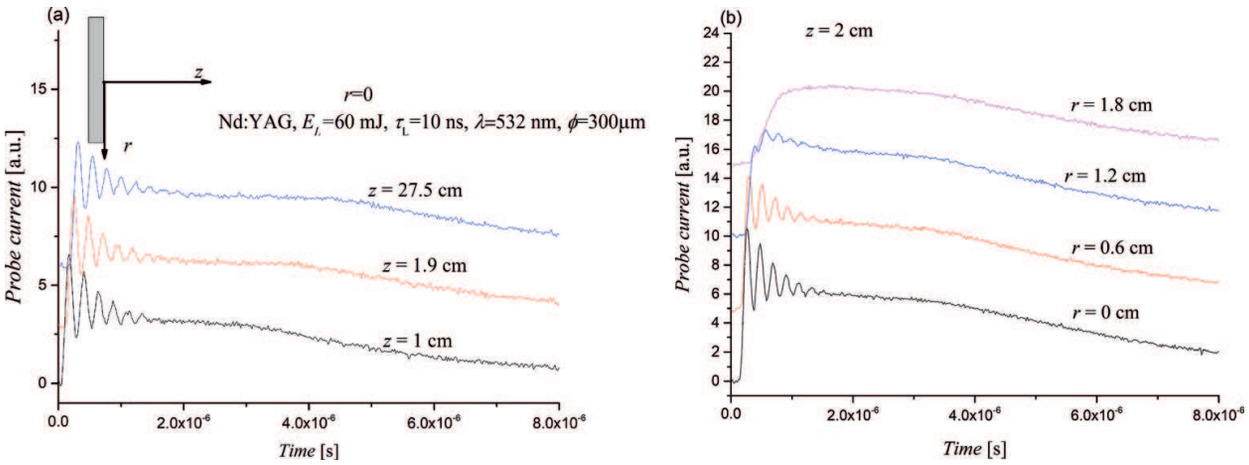

Figure 2. Typical time-dependence of the ionic current recorded by the Langmuir probe (biased at V_P = −30 V) placed at various axial (a) and radial (b) distances from the center of the laser irradiation spot (Al target, ns ablation [55]).

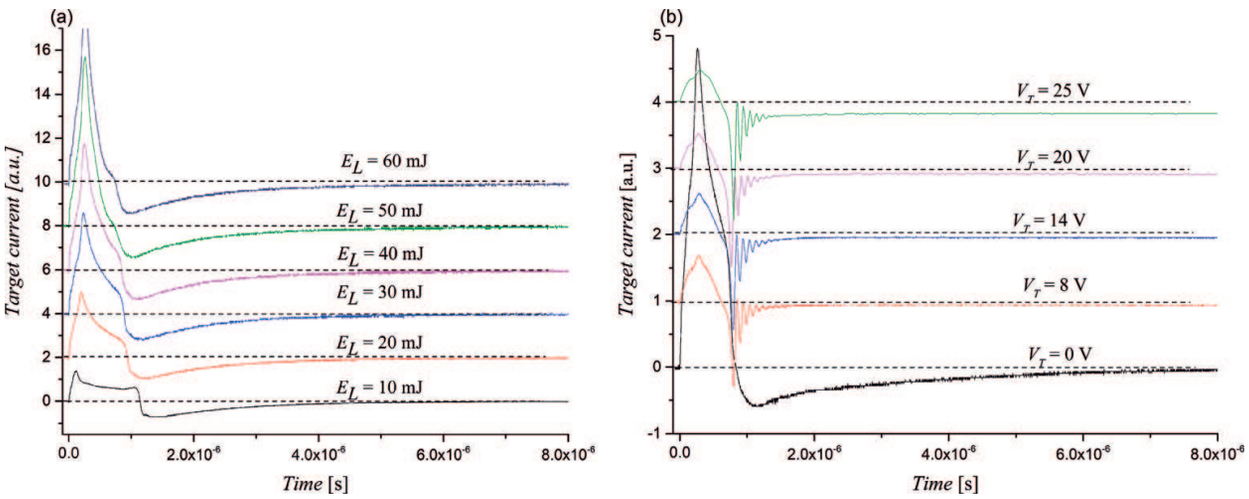

Figure 3. Currents induced in the ns-irradiated target (Al) for (a) various laser beam energies (V_T = 0 V) and (b) target biases (E_L = 60 mJ/pulse).

through the electrons escaping from the expanding plasma to the grounded chamber, while the negative charging is given by the ions escaping from the target. The asymmetry of the laser intensity distribution and non-uniform target absorptivity can also lead to the generation of considerable currents along a conductive target [85]. Experiments revealed two possible mechanisms: induction due to the magnetic dipole moment of the plasma and a second mechanism resulting from the phenomena at the plasma-target interface [85–87]. From these experimental results, we observed that the amplitudes of the fast peak increase rapidly with the laser energy and the fast electron contribution becomes dominant above E_L = 16 mJ/pulse (~20 J/cm^2 fluence) [65]. Biasing the target (V_T) by an external voltage stabilized source, the negative part of the target current, which is given by the ion contribution, acquires an oscillatory behavior of the same frequency as previously recorded for the Langmuir probe current (**Figure 3b**). We therefore deduced that such periodic fluctuations were induced by the probe/target electric field, with a target bias threshold for their occurrence.

When extracting the oscillatory part from the original signal (**Figure 2**), that is, subtracting the smoothed temporal trace, the resulted time-dependence revealed a good fitting with a usual damp oscillator [48, 60]. Thus, one can assume that in the electric field near the probe the ion equation of motion is $\ddot{x} + \nu_{ei}\dot{x} + \omega_{pi}^2 x = 0$, where the dissipative term is given by the electron-ion collision frequency, $\langle \nu_{ei} \rangle \sim 1.5 \times 10^{-6}\ z^2 n_e \ln\Lambda / T_e^{3/2}$ [Hz], and $f_{pi} = \omega_{pi}/2\pi = 210z\sqrt{n_i/A}$ [Hz] is the plasma ion frequency [49, 60]. We applied this procedure also for studying the LP current oscillations in the case of fs-laser ablation of Al. In a more detailed analysis, we observed that biasing the target can influence the oscillation frequency, two regimes being observed, corresponding to the fast and slow components, respectively. For example, in **Figure 4a** and **b** we observed good fitting for V_T = +1.6 V and V_T = +35 V, resulting in oscillation frequencies υ = 8.37 MHz and υ' = 6.46 MHz. For an intermediate value, V_T = +19.5 V, we distinguished two parts: (i) at short recording times (<400 ns), a fast plasma structure oscillating with a frequency of υ = 8.93 MHz, which is similar with the previous value for V_T = +1.6 V; (ii) a slow structure for longer times (>400 ns), oscillating with a frequency of υ' = 6.74 MHz, which is similar with the previous value for V_T = +35 V. This is in good agreement with the existence of two types of particles, that is, plasma structures, which are formed during the initial expansion process: a fast (hot) one consisting in highly charged particles promptly ejected in an expansion process characterized by the acceleration through the electric field given by initial charge separation (ambipolar diffusion); and a slow (cold) tail consisting in thermalized particles with low average charge state. Such double-structures are often reported in the literature for both fs- and ns-laser ablation, being observed for plume propagating in an ambient gas [14, 15, 20, 88] and in vacuum for high-fluence irradiation [56, 57, 67, 75]. Reports from literature usually present a difference of one order of magnitude between the expansion velocities of the two plasma components. The Fourier transform of the probe current (**Figure 4c**) confirms the existence of two oscillatory regimes, through the existence of two peaks which are evidenced differently at various target voltages. Their frequencies are plotted in **Figure 4d** vs. V_T as obtained from the above-mentioned sine damp fitting and from the Fourier transform, respectively. Let us observe that both methods gave similar results, two groups being computed with average values υ = 8.5 MHz and υ' = 6.5 MHz.

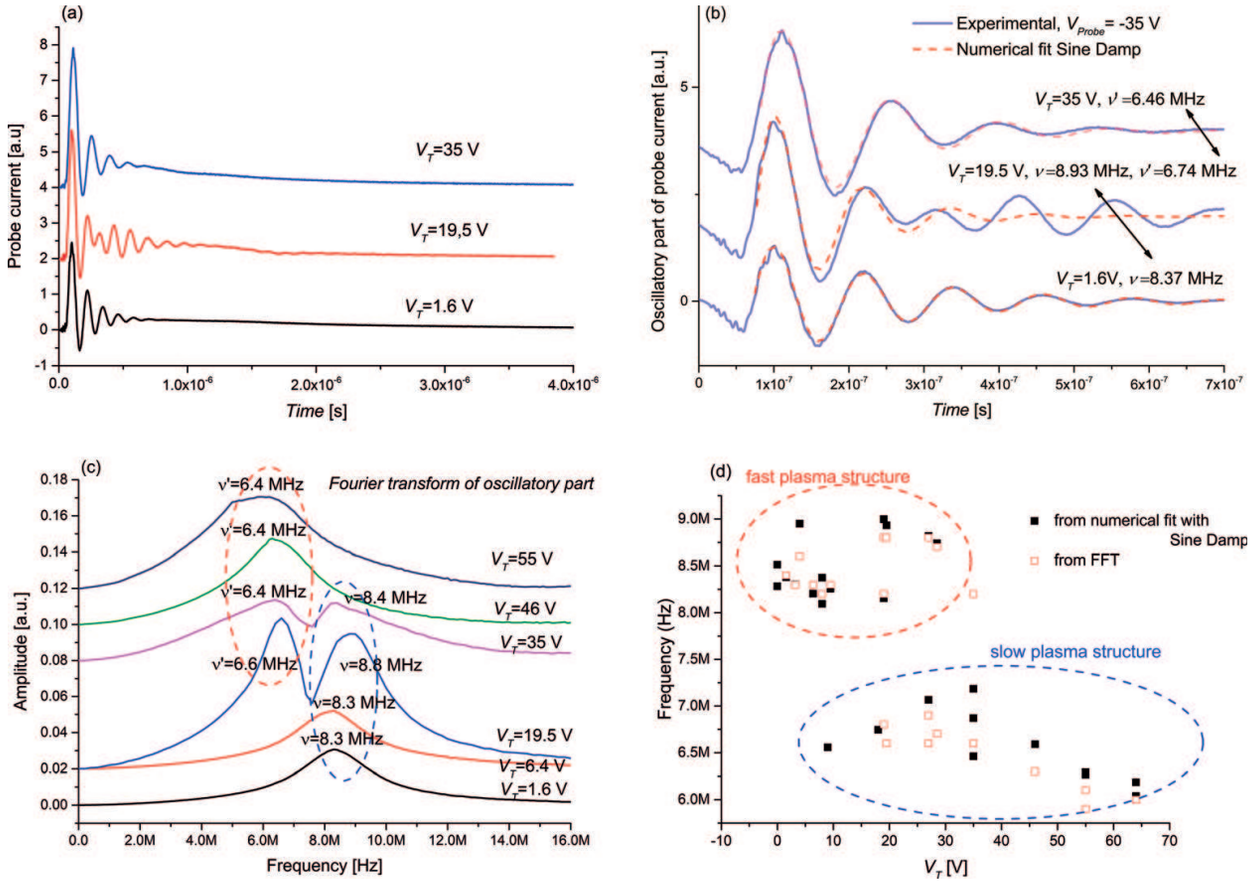

Figure 4. Typical temporal evolution of the current recorded by the negatively biased probe, $V_P = -35$ V (a), oscillatory part obtained by smoothing the temporal trace and subtracting from the original one (b), its Fourier transform (c) and frequencies obtained for various target biasing V_T (d), for Al fs-laser-produced plasma.

There is no clear dependence of the oscillation frequencies on the probe biasing, their variations being in the limits of the determination error bars. A similar behavior was observed when using a Cu target: at short recording times, the probe current oscillates with a frequency of υ = 10.5 MHz, while it shifts later to υ' = 6.4 MHz, the values being averaged over the various target biases. Moreover, both oscillating regimes are observed in the probe current regardless of probe biasing, the behavior being slightly different when compared with the case of Al target, where they occurred only for intermediate values V_T = +(19–35) V.

During these measurements, a discussion has arisen on the use of low or high oscilloscope impedance for recording the transient signals. Both configurations have advantages and disadvantages. Using low impedance ensures good temporal resolution, while using a high input impedance has the advantage of improving the signal amplitude, although the temporal trace $i(t)$ is artificially extended through its convolution with the apparatus function,

$$i_C(t) = \int_{-\infty}^{\infty} i(\tau)h(t-\tau)d\tau \tag{1}$$

where t is the time and $h(t)$ the convolution function, which for our experiments was of exponential decay type, $h(t) = \exp(-t/\tau_0)$, with $\tau_0 = 16 \times 10^{-6}$ s, the time constant deduced from

the electrical circuit parameters. In such experimental conditions, the probe current is given in **Figure 5a**, where we can observe that the oscillations are preserved at short recording times, since the convolution of a periodic function is also periodic. However, through the inverse mathematical procedure, the numerical deconvoluted signals fit well with the probe current recorded using a low oscilloscope input impedance. For example, in **Figure 5b** such comparison is made for Al targets and $V_T = 0$, $V_P = -30$ V. We therefore used one or the other configuration, with easy conversion between them through convolution/deconvolution procedures.

The consequence of applying a positive voltage on the metallic target, $V_T = +35$ V, is the appearance of an initial hump at short recording times (see **Figure 6a**). Such biasing is influencing the plasma expansion at the initial stages by accelerating the ions and retarding the electrons. Therefore, an excess of fast positive electric charges results, in the form of a residual ionic current. The fast plasma structure acceleration is given by the ambipolar electric field within a thin layer in the plume periphery, where quasi-neutrality of the plasma is broken [34], and the resulting double layer is influenced by the target biasing, at the early stages of

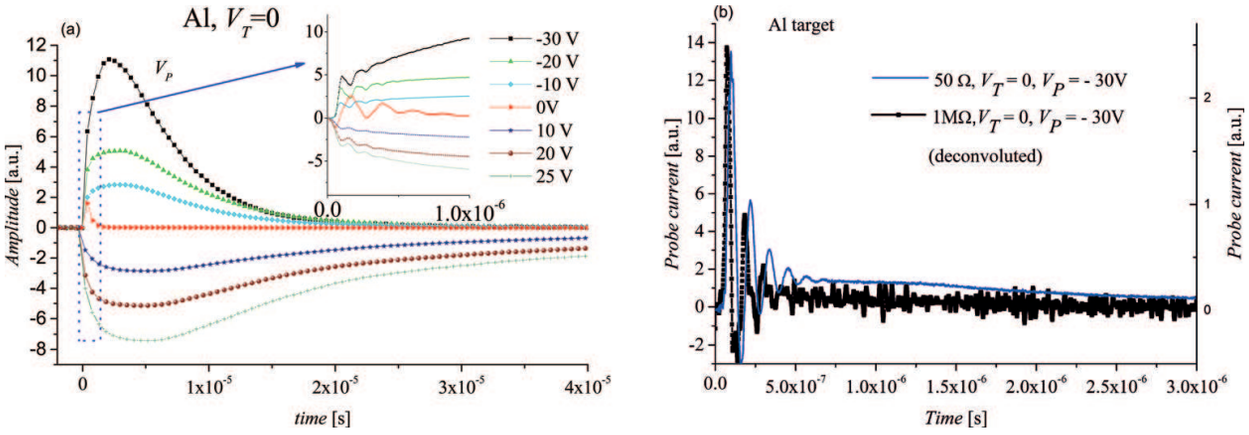

Figure 5. Typical temporal profiles of the current recorded by the LP probe at 3.5 mm from the target and various values of the probe biasing voltages: Al target, fs-laser ablation, high input impedance (a) and numerically deconvoluted signal compared to the current recorded using a low oscilloscope input impedance (b).

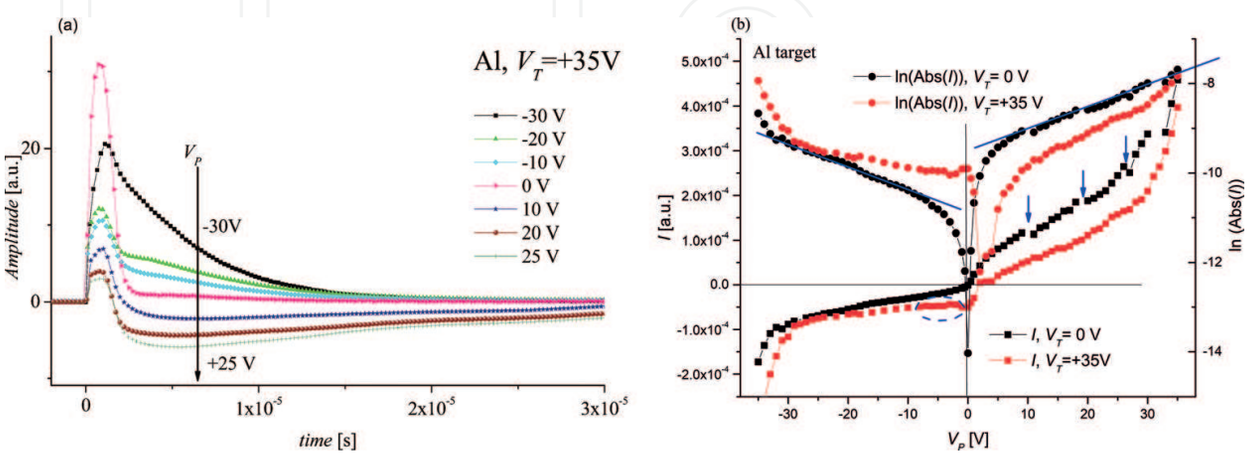

Figure 6. LP current temporal profile for positive target biasing, $V_T = +35$ V, at various probe biasing voltages (a) and total collected charge versus probe potential in linear and semi-logarithmic coordinates (b): Al target, fs-laser ablation, high input impedance.

expansion. The time-extension of the initial hump is longer in the case of higher atomic mass targets and it indicates a dependence on the inertial properties, the light ions being faster repelled by the positively biased target. These measurements can be successfully used to calculate the global temperature and average charge state for the fast plasma structure, by time-integration of probe current intensity to obtain the total collected charge dependence versus probe potential (**Figure 6b**). It was observed that for both electronic and ionic branches, corresponding to positive or negative LP biasing, for small values of the probe potential ($|V_P| < 10$ V), the dependence is of $\sqrt{|V_P|}$ type. This is given by the repelling/attracting of charges from the cold (slow) structure, and it shows a saturation trend as the potential increases because the slow structure center-of-mass velocity is easily influenced by the probe field. Between ±10 and ±35 V, an exponential dependence results, the collected charge is mainly influenced by the behavior of the hot (fast) plasma structure and a semi-logarithmic plot (**Figure 6b**) shows a linear dependence. The positive exponential branch corresponding to the fast electrons allows the computing of electron temperatures from the slope of the semi-logarithmic representation, the resulting values being time-averaged. Moreover, in the assumption of an isothermal plasma, taking also into account the ionic branch, the average ion charge state can be derived as the ratio of the two regions slopes. The results are given in **Table 1** for various metallic targets. We observed that a high positive correlation exists between the deduced average charge states and the plasma temperatures. This result is in agreement with plasma standard theoretical models, for example, local thermodynamic equilibrium or collisional radiative [89], where average charge state or ion fractional populations can be easily computed in the case of a homogenous plasma, for given electron temperature and atom density (e.g. see **Figure 5** of [90]).

Another approach used by our group is based on the treatment of the current-voltage characteristics (*I-V* plots) derived from the time-of-flight current profiles recorded at various probe biases and sampled at specific delays after the laser pulse [77]. In principle, this "classical" method [40, 91–93] considers only the thermal movement of the particles (without streaming) and a Maxwellian distribution function. Space-time evolution of electronic temperature, thermal velocity, plasma potential and particle density can be derived from the *I-V* characteristic based on the results of the "classical" LP theory. In the framework of the LP method, all main plasma parameters are derived from the electronic part of the *I-V* characteristic:

Target	Atomic weight	T_e (eV)	Average charge state (z)
Al	27	14.21 ± 2.15	2.63 ± 0.74
Mn	55	8.15 ± 0.79	1.08 ± 0.42
Ni	59	6.72 ± 1.03	1.29 ± 0.37
Cu	64	6.54 ± 0.45	1.59 ± 0.23
In	115	8.66 ± 1.29	2.23 ± 0.94
Te	128	8.04 ± 0.84	1.44 ± 0.24
W	184	5.29 ± 0.53	0.92 ± 0.17

Table 1. Plasma temperature for various metallic targets.

http://dx.doi.org/10.5772/intechopen.70759

$$I_{Probe} = I_{e0}\exp\left[-e(V_{Plasma} - V_{Probe})/k_B T_e\right] \quad - \quad I_{i0}, \quad V_{Probe} < V_{Plasma} \tag{2}$$

where I_{Probe} is the probe current, I_{e0} and I_{i0} are the electron and ion saturation currents, V_{probe} is the bias applied on the probe, V_{Plasma} is the plasma potential, e is the electron charge, k_B is the Boltzmann constant, T_e is the electron temperature.

The electron temperature (T_e) can be further determined from the slope of the semi-logarithmic plot of the probe current from the saturation region (I_e) versus probe bias (V_p), the plasma potential (V_{Plasma}) representing the inflection point separating the linear increase from the saturation region, while the ion density and thermal velocity are given by the following equations:

$$I_{i0} = \frac{1}{4} e A n_i \sqrt{\frac{8k_B T_i}{\pi m_i}} \tag{3}$$

$$v_{thermal} = \frac{1}{4} \sqrt{\frac{8k_B T_i}{\pi m_i}} \tag{4}$$

where A is the probe collecting area, n_i is the ionic density, m_i is the mass of the particle and T_i the ion temperature which is considered to be equal to the electron temperature, assuming the local thermodynamic equilibrium (LTE) hypothesis.

We applied this particular method to study the dynamics of the plume at relatively long delays (>1 μs) after the laser pulse. Based on our previous ICCD fast camera imaging and space- and time-resolved optical emission spectroscopy measurements, we know that these times are characteristic for the observation of the slow plasma component [55, 56, 67]. As expected, it resulted that all studied parameters have a significant space-time decrease, due to the cooling process and rarefaction during expansion (**Figure 7**). Comparing the values for the electron temperatures determined using time-sampling methods with the ones given by the previous method, some notable differences occur. The time-resolved method only captures the cold tail arriving at the probe surface as the sampling is done after 1 μs, and thus the values of the

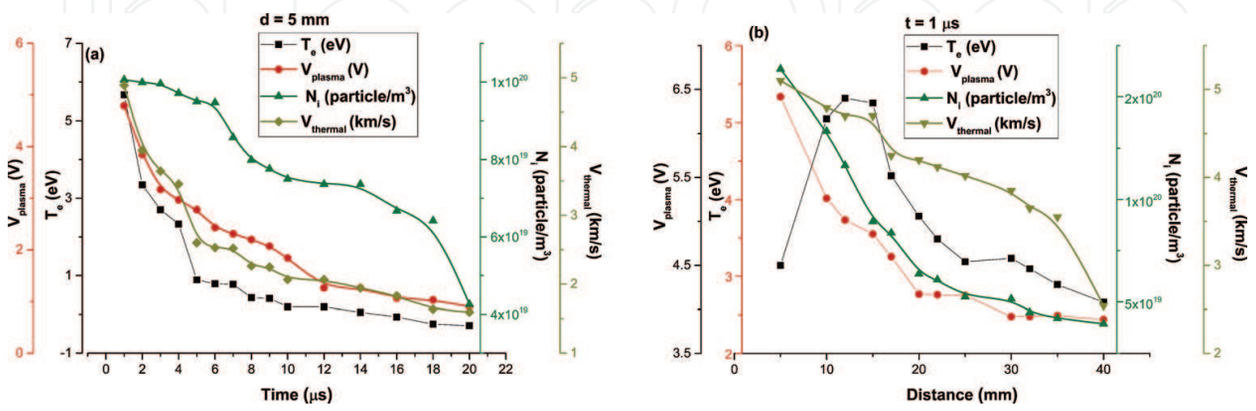

Figure 7. T_e, V_{plasma}, n_i and $v_{thermal}$ dependence on (a) time at a fixed distance (d = 5) and (b) space for a fixed moment in time (t = 1 μs), derived for an Al plasma generated by ns laser ablation.

electron temperatures are considerably lower than the ones derived from the total collected charge versus probe potential representation.

The same technique has been implemented for the study of transient plasmas generated by laser ablation in three different temporal regimes (ns, ps, fs) on a series of six metallic targets (Al, Ti, Mn, Ni, Cu, Zn). **Figure 8a** shows the decrease of the saturation ion density (recorded at 5 mm from the target and after 1 μs with respect to the laser pulse) with the melting point of the target material. Other groups have reported similar evolutions for ns-laser-produced plasmas. A significant decrease of the ablation efficiency (estimated as a function of the ablated crater depth) with the increase of the melting point was reported in [94]. A similar influence of the melting point on the ablation yield was found by Schou et al. [29, 95], who discussed the decrease in the ablation yield as a consequence of the target cohesive energy increase. Both melting point and cohesive energy are considered as a measure of the degree of volatility. The same dependence proposed by previously mentioned authors was also found by our group for fs-laser ablation of various metallic targets (W, Te, In, Cu, Ni, Mn, Al) [77]. The decrease of the ionic density with the increase of the melting point (or cohesive energy) appears to be a general characteristic of the laser-produced plasmas as it is confirmed by our current systematic study on the ns, fs and ps ablation for a wide range of metallic targets.

Figure 8b displays the evolution of the electronic temperature with the target electrical conductivity for the three ablation regimes. The values derived at $t = 1$ μs and $d = 5$ mm present a steep increase for low conductivity elements reaching a quasi-saturation regime after 10 MS/m. The experimental data were fitted with the same function [77] for the three ablation regimes: $T(\sigma) = c_T - \frac{b_T}{\sigma + a_T}$ where a_T, b_T, c_T are constants, characteristic for each ablation regime. Considering the wide range of target conductivities, spanning approximately two orders of magnitude from 0.62 MS/m for Mn to 59 MS/m for Cu, and the values of the electronic temperature (1–9 eV, commonly encountered for plasmas generated by laser ablation at low-moderate fluence), a generalization is somehow appealing. However, we note that these particular values characterize only a particular plasma volume investigated at a specific moment in time

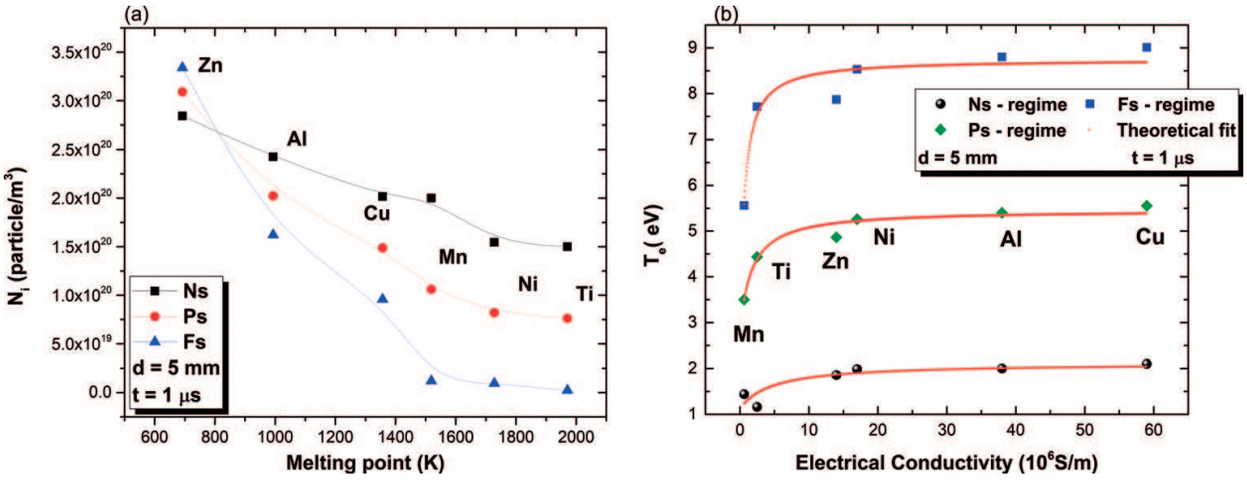

Figure 8. (a) Ion density dependence on the target melting point for three ablation regimes (ns, ps and fs) and (b) the electronic temperature dependence on the electrical conductivity of the metallic targets.

(1 μs delay and a distance of 5 mm from the target) and further investigations are thus required to establish the universality of the proposed dependence.

Let us note that in the results presented above only single-element targets were used to better understand the fundamental processes involved in laser-target interaction and subsequent plasma evolution. When using complex (multi-component) targets, the interpretation of the LP temporal profiles is more difficult. For example, we present in **Figure 9** the results for laser ablation of a chalcogenide glass ($Ge_{9.5}Sb_{28.6}Se_{61.9}$) [75], where three plasma structures are recorded, each of them oscillating with a specific frequency. These structures are also present in ICCD images (see the inset of **Figure 9**), displaying various expansion velocities.

An extensive investigation of plasmas generated by ns laser ablation of chalcogenide targets was presented in [75]. We reported there a strong evolution of the global expansion velocity of all three plasma components (derived from ICCD fast camera imaging) and of the excitation temperatures (determined through optical emission spectroscopy) with the thermal and electrical properties of the complex chalcogenide target. More precisely, the increase of the Sb_2Se_3 content led to a quasilinear increase of the expansion velocities and average plasma temperature. The results were interpreted in the frame of the target structural changes. Previous reports on the properties of similar systems revealed that the addition of Sb leads to the decrease of the bandgap energy [96], the increase of the glass transition temperature and

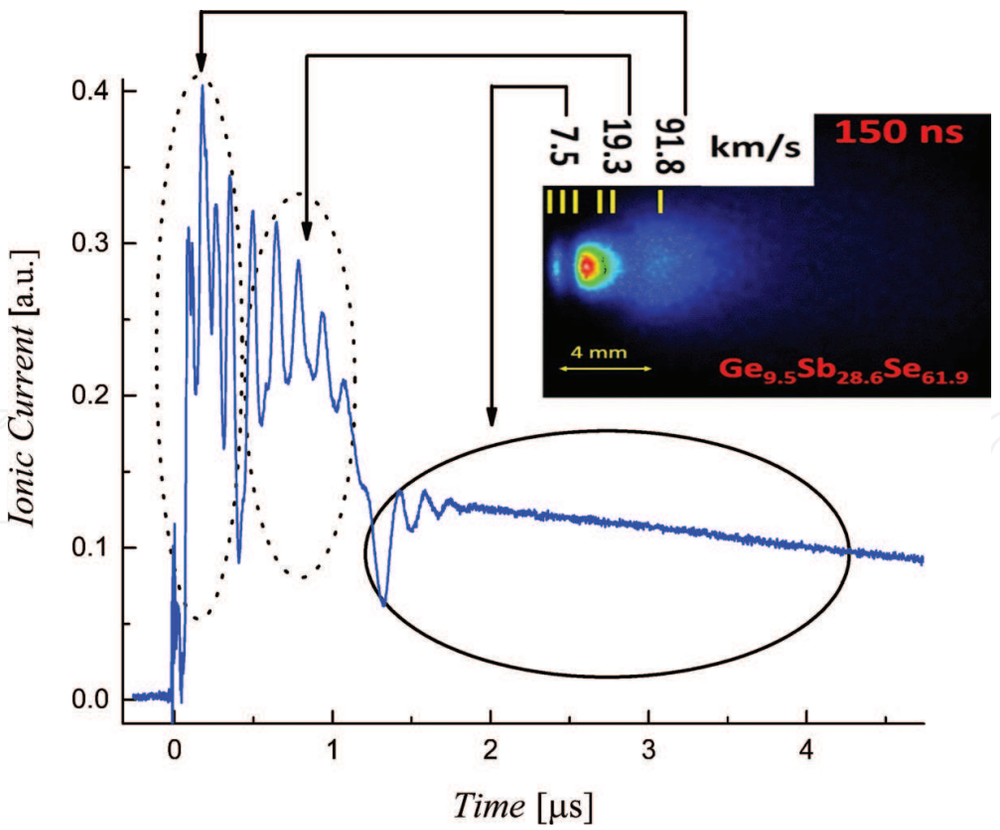

Figure 9. LP current for fs-laser-produced plasma using a chalcogenide glass target and ICCD image (inset) showing the occurrence of three plasma structures.

consequently the increase of the weak bonds concentration [97]. The increase in the weak bonds concentration leads to increase in the thermal and electrical conductivity of the glass. This is in good agreement with our reported results on pure metallic targets [77], where the increase in the electrical/thermal conductivity of the materials led to the increase of electron temperatures and ion drift velocities.

4. Theoretical investigations

Continuing our previous work [55, 58, 59, 63] on the fractal hydrodynamic model for laser ablation plasma dynamics, we recently proposed a compact version for the analysis of the spatial and temporal evolution of some plasma dynamic variables [76]. This version of our model was obtained by using normalized variables of the particle density, velocities, current density, etc., and by choosing adequate scale resolutions. In our initial model describing the evolution of the fractal fluid [59, 63, 98], we took into account a high number of factors (experimental ones by means of the width of the laser pulse Gaussian distribution, probe or target bias, etc., and theoretical ones by means of the fractal-non-fractal transition coefficient, resolution scale, fractal dimension of the movement curves, etc.), which increased the difficulty in performing a complete analysis of the plume dynamics. Through a viable choice of normalized dynamic variables with respect to the previous factors, we simplified the interpretation of the plume dynamics.

In the frame of fractal hydrodynamics with an arbitrary fractal dimension of the motion curves, D_F, we obtained for the one-dimensional case in absence of an external potential the specific momentum and density conservation laws [59, 63, 98]:

$$\partial_t v + v\partial_x v = -2\lambda^2 (dt)^{\left(\frac{4}{D_F}\right)-2} \partial_x \left(\rho^{\frac{-1}{2}} \partial_{xx} \rho^{\frac{-1}{2}}\right) \tag{4a}$$

$$\partial_t v + \partial_x (\rho v) = 0 \tag{4b}$$

with v the velocity, ρ the density, dt the scale resolution and λ a fractal-non-fractal transition coefficient. Using the method presented in [59, 63], the analytical solutions for Eqs. (4a) and (4b) are

$$v(x,t) = \frac{c\alpha^2 + \left[\frac{2\lambda(dt)^{(2/D_F)-1}}{\alpha}\right]^2 xt}{\alpha^2 + \left[\frac{2\lambda(dt)^{(2/D_F)-1}}{\alpha}\right]^2 t^2} \tag{5}$$

for the velocity field and

$$\rho(x,t) = \frac{\pi^{-1/2}}{\left\{\alpha^2 + \left[\frac{2\lambda(dt)^{(2/D_F)-1}}{\alpha}\right]^2 t^2\right\}^{1/2}} \cdot \exp\left\{\frac{-(x-ct)^2}{\alpha^2 + \left[\frac{2\lambda(dt)^{(2/D_F)-1}}{\alpha}\right]^2 t^2}\right\} \tag{6}$$

for the particular initial and boundary conditions given by:

$$v(x, t = 0) = c, \quad \rho(x, t = 0) = \rho_0 e^{(-x/\alpha)^2} \tag{7}$$

$$v(x = ct, t) = c, \quad \rho(x = -\infty, t) = \rho(x = \infty, t) = 0 \tag{8}$$

Thus, we assumed that at $t = 0$ the center of the initial Gaussian distribution ρ is located at x $(t=0)>0$ and has the velocity $v(t=0)>c$. This is supported by the fact that the laser beam temporal profile is usually of Gaussian type, and consequently we can consider a similar distribution of the plasma plume along the expansion direction. Moreover, if the plasma parameters are investigated at time scales longer than the laser pulse width, one can also assume that the particles are ejected with a constant expansion velocity. In this approximation, a correlation could be established between the density distribution of the ejected particles and the laser pulse temporal distribution [55] (in the hypothesis of total laser energy absorption by the plasma plume). A similar outcome is obtained for $<x> = ct$. From such a perspective, with respect to the movement plane of any particle ($<x> = ct$) of the ablation plasma at any time $\neq 0$, the velocities of the ejected particles are constant during expansion (Eq. (8)) and the density becomes null at large distances from the target. By means of the conditions:

$$t \gg \frac{\alpha^2}{2\lambda(dt)^{\left(\frac{2}{D_F}\right)-1}} \tag{9a}$$

$$x \ll \frac{c\alpha^2}{2\lambda(dt)^{\left(\frac{2}{D_F}\right)-1}} \tag{9b}$$

the current density takes the approximate form:

$$j(x,t) = v(x,t)(x,t) = \pi^{-1}\frac{c}{\alpha}\left[\frac{\alpha^2}{2\lambda(dt)^{\left(\frac{2}{D_F}\right)-1}}\right]^2 \frac{1}{t^3} \times \exp\left\{-\left[\frac{\alpha^2}{2\lambda(dt)^{\left(\frac{2}{D_F}\right)-1}}\right]^2 \left(\frac{x}{t} - c\right)^2\right\} \tag{10}$$

which is similar with a shifted Maxwellian distribution [99, 100], often used for treating the temporal trace of the LP current:

$$j(t)\frac{1}{t^3}\exp\left[\frac{-m}{2k_B T_{ionic}}\left(\frac{d}{t} - v_{drift}\right)^2\right] \tag{11}$$

through the following identities:

$$x \equiv d,\ v_{drift} \equiv c,\ \frac{m}{2k_B T_{ion}} \equiv \left[\frac{\alpha^2}{2\lambda(dt)^{\left(\frac{2}{D_F}\right)-1}}\right]^2 \tag{12}$$

Given the dependences of the multiple dynamic variables (ρ, v, j, etc.) on the external factors ($ex : \alpha, \lambda, (dt)^{\left(\frac{2}{D_F}\right)-1}$, etc.), we choose an adequate normalization that will allow us to obtain more compact and simplified dependences. Basically, we want to reduce the explicit dependences on the external factors. Thus, by means of the condition $2\lambda = \alpha c$, we will choose the normalization:

$$\xi \rightarrow \frac{x}{\alpha}, \tag{13a}$$

$$\tau \rightarrow \frac{tc}{\alpha}, \tag{13b}$$

$$\mu \rightarrow (dt)^{(4/D_F)-2} \tag{13c}$$

This allows us to re-write the dependencies of the plasma dynamic variables on the external factors as follows [76]:

Normalized velocity:

$$V(\xi, \tau, \mu) = \frac{1 + \mu\xi\tau}{1 + \mu\tau^2} \tag{14}$$

Normalized particle density:

$$N(\xi, \tau, \mu) = \left[1 + \mu\tau^2\right]^{-1/2} \cdot \exp\left[\frac{-(\xi - \tau)^2}{1 + \mu\tau^2}\right] \tag{15}$$

Normalized current density:

$$J(\xi, \tau, \mu) = \frac{1 + \mu\xi\tau}{\left[1 + \mu\tau^2\right]^{3/2}} \cdot \exp\left[\frac{-(\xi - \tau)^2}{1 + \mu\tau^2}\right] \tag{16}$$

Let us analyze the influence of the μ parameter (named fractalization degree) which contains the contribution of all external factors, by means of the fractal-non-fractal transition coefficient, λ, and scale resolution, dt and fractal dimension, D_F, of the movement curves. From a physical perspective, fractalization implies different statistics (from Levy-type movements to Brownian movements, either by means of non-Markovian processes or Markovian ones [63, 98]) that are imposed by the fundamental processes involved in the plasma formation and expansion. In such context, we assumed that generally for laser ablation there are two main mechanisms responsible for the formation and expansion of two plasma structures [15, 16, 56, 67, 73, 80–82], which were previously experimentally evidenced. Thus, the first structure is a result of the electrostatic interactions, at very short time scale, the positive charge left on the target surface by electron laser excitation and detachment would accelerate the positive ions outwards the surface (Coulomb mechanism [13]). The second plasma structure that requires more time to form and expand is generated through thermal mechanisms (evaporation, phase explosion

http://dx.doi.org/10.5772/intechopen.70759

[101]). Each mechanism is characterized in our model by a specific scale resolution, that is, an adequate choice of the fractalization degree, μ.

In this context, in **Figure 10a** and **b** the current densities given by Eq. (16) are plotted versus time (τ) for various normalized distances (ξ) and fractalization degrees: $\mu = 0.3$ (a) and $\mu = 7$ (b). Such distinct evolutions are associated with the two plasma structures, while their overlapping fits well the experimental LP temporal trace given in **Figure 2**, except the current oscillations which should be treated separately. The space-time evolution of the variables describing the plasma is in agreement with other theoretical models [102, 103]. Moreover, having in view the normalization used in our model, it is possible to control some dynamics of the plasma plume by means of the fractalization degree μ.

The validation of our model comes from the comparison with the time-dependence of plasma parameters obtained from LP measurements. In **Figure 11a** one observes that the time-decrease of the ion density is well fitted by the dependence (15), with the parameters

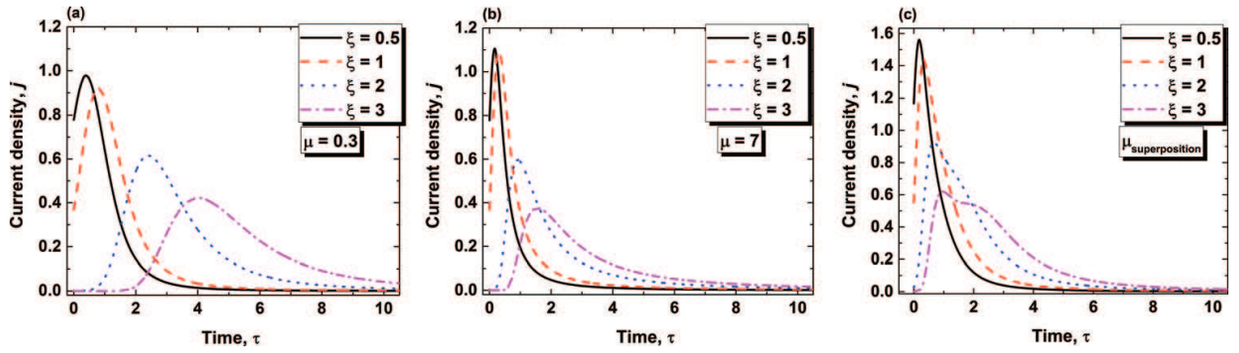

Figure 10. Current densities given by Eq. (16) dependence versus time (τ) for various normalized distances (ξ) and fractalization degrees: $\mu = 0.3$ (a) and $\mu = 7$ (b) and their overlapping (c).

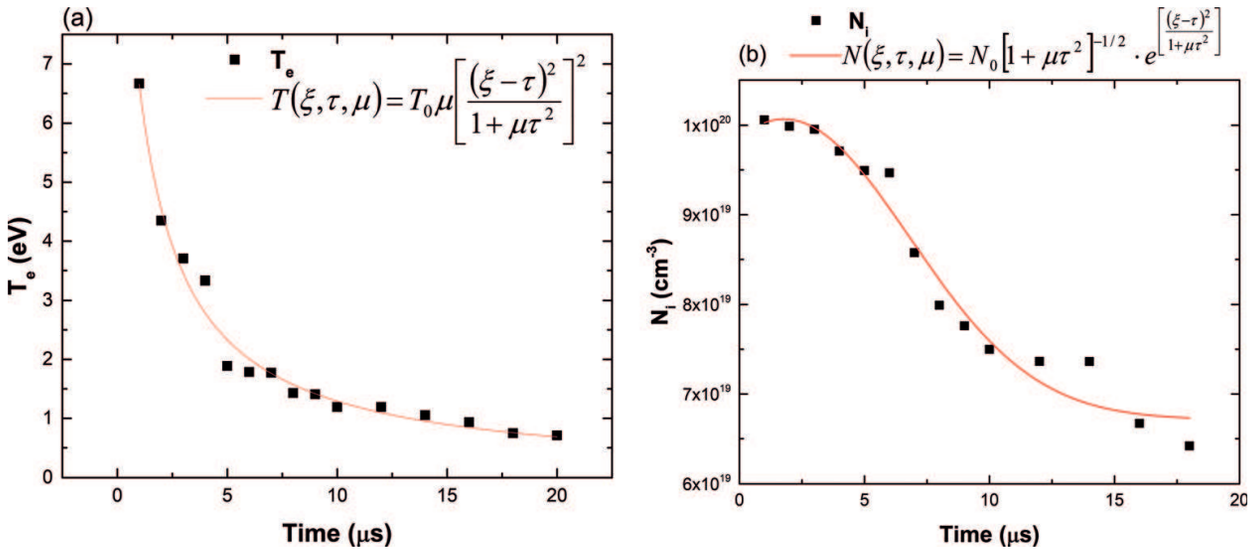

Figure 11. Experimental (squares) temporal evolution of the ion density (a) and electronic temperature (b), and individual fits (continuous line) using the relationships extracted from the compact fractal hydrodynamic model [76].

$N_0 = 4.25 \times 10^{19}$ cm^{-3}, $\xi \sim 11.8$, $\mu \sim 2.95$, where N_0 is a normalization constant. Moreover, the right term of Eq. (4a) is the space derivative of a fractal potential,

$$Q = 2\lambda^2 (dt)^{\left(\frac{4}{D_F}\right)-2} \rho^{\frac{-1}{2}} \partial_{xx} \rho^{\frac{-1}{2}} \tag{17}$$

Then, using Eq. (17) and the normalizations (13a)–(13c), the fractal potential takes the normalized form:

$$q(\xi, \tau, \mu) = \mu \left[\frac{(\xi - \tau)^2}{1 + \mu\tau^2} \right]^2 \tag{18}$$

In the "classical" LTE model, the plasma temperature (T) is a measure of the thermal movement (described by the random movement of the plasma ions, electrons and neutrals), property which is reflected here by the plasma particles motion curves non-differentiability. In our model, since the fractal potential (q) is a measure of non-differentiability, this leads to a relation of proportionality between the two dynamic variables ($q \sim T$). In such context, we observed that the dependence (18) fits well the time evolution of the electronic temperature (**Figure 11b**), with the parameters $T_0 = 0.68$ eV, $\xi \sim 11.5$, $\mu \sim 2.8$, where T_0 is a normalization constant.

The normalization of the plasma dynamic variables led us to a more compact and simple form of the fractal theoretical model, by allowing the use of a single control parameter that embodies the contributions of several external parameters on the dynamics of the ejected particles. In its compact form, we were able for the first time [76] to define some clear associations between fractal model variables and specific plasma parameters (electron temperature, thermal velocity, particle density). Moreover, when compared with experimental data depicting the temporal evolution of the plasma parameters determined though the Langmuir probe method, the model satisfactorily reproduces the experimental traces. From the theoretical fit, we determined a range of values for the fractalization degree which describes the laser-produced plasmas in the ns ablation regime. The success of this non-differential approach is also seen from the fact that the model is able to "recognize" the probe—target distance at which the experimental data was recorded. Further studies are required in order to test the generality of the model, by comparing it against other "classical" theoretical models and also against data extracted from ps and fs laser-produced plasmas in various experimental conditions (target-probe distance, laser fluence, background pressure).

In the classical concepts, the theoretical models (hydrodynamic, kinetic, etc.) are built assuming that the dynamics of individual elements are characterized by continuous and differentiable motion variables (energy, momentum, density, etc.). These variables are exclusively dependent on the spatial coordinates and time. In the real situation, the complex system dynamics is much more complicated and the classical theoretical models failed in the attempt to explain all the concerned aspects. These difficulties can be overcome in a complementary approach, using fractal concepts, describing "exotic" shapes that did not fit the patterns of

http://dx.doi.org/10.5772/intechopen.70759

Euclidean geometry. Moreover, the depth analysis of different complex systems evolution showed that most of the phenomena are nonlinear and, therefore, new mathematical tools were required. These have been provided by the Scale Relativity Theory (SRT) and by Extended Scale Relativity Theory (ESRT) [98], that is, the SRT with an arbitrary constant fractal dimension. These theories consider that the motions of the complex systems structural units take place on continuous but non-differentiable curves (fractal curves). In this situation, Euclidean dynamics of a complex system subjected to external constraints is replaced by a fractal dynamics characterizing the same system free of any external constraints. More precisely, Euclidian constraints dependent motions, that is, on continuous but differentiable curves, are substituted by constraints independent motion in a fractal space, that is, on continuous but non-differentiable (fractal) curves (a free motion).

5. Conclusions

The dynamics of the transient laser-produced plasma in vacuum was investigated using electrical (Langmuir probe, target current) and optical (fast gate intensified CCD camera imaging) measurements for various ablation regimes and simple target materials. The typical time-evolution of the ion current recorded by the probe placed at various distances (axial, radial) with respect to the center of the laser irradiation spot shows that it extends in the μs range, and it generally consists in a fast part having an oscillatory behavior, and a slower tail which arrives at longer times. For the expansion velocities, values in the range of 10^4 m/s for the first (fast) structure and of 10^3 m/s for the second (slow) one were found, both from electrical and optical methods, which are in agreement with experimental results given in the literature and rough calculations performed in simple thermodynamic framework.

Measurements of the current induced in the target by the ablation process showed that it is correlated with the probe signal, as the positive charging arises through the electrons escaping from the expanding plasma to the grounded chamber, while the negative charging is given by the ions escaping from the target. Biasing the target by an external voltage source, the negative part of the target current, which is given by the ion contribution, acquires an oscillatory behavior of the same frequency as previously recorded for the Langmuir probe current. Consequently, such periodic fluctuations are assumed to be induced by the probe/target electric field, with a target bias threshold for their occurrence.

Extracting the oscillatory part from the original temporal trace of Langmuir probe, the resulted time-dependence revealed a good fitting with a usual damped oscillator, while its frequency is connected with the plasma ion frequency. Moreover, we observed that biasing the target can influence the oscillation frequency, two regimes being inferred, corresponding to the fast and slow components, respectively.

Electrical measurements can be successfully used to calculate the global temperature and average charge state for the fast plasma structure, through time-integration of probe current intensity to obtain the total collected charge dependence *vs*. probe potential. We observed a high positive

correlation between these two parameters, the result being in agreement with plasma standard theoretical models (e.g. local thermodynamic equilibrium or collisional radiative).

Another approach used by us to study the dynamics of the plume at relatively long delays is based on the treatment of the current-voltage characteristics (*I-V* plots), that are derived from the time-of-flight current profiles recorded at various probe biases and sampled at specific delays after the laser pulse. Space-time evolution of electronic temperature, thermal velocity, plasma potential and particle density were computed, all of them having a significant decrease, due to the cooling process and rarefaction during expansion. The technique has been implemented for the study of transient plasmas generated by laser ablation in three different temporal regimes (ns, ps, fs) on a series of six metallic targets (Al, Ti, Mn, Ni, Cu, Zn). A decrease of the ionic density with the increase of the melting point (or cohesive energy) is observed, and it appears to be a general characteristic of the laser-produced plasmas, as it is confirmed by our current systematic study on the ns, fs and ps ablation for a wide range of metallic targets. The evolution of the electronic temperature with the target electrical conductivity for the three ablation regimes presents a steep increase for low conductivity elements, reaching a quasi-saturation regime after 10 MS/m. However, the obtained values characterize only a particular plasma volume investigated at a specific moment in time, and further investigations are required to establish the universality of the proposed dependence.

Theoretically, a compact version using normalized variables of our previous fractal hydrodynamic model was proposed for the analysis of the spatial and temporal evolution of some plasma dynamic variables. In this context, a new parameter named fractalization degree was introduced to account for the contribution of all external factors, that is, the fractal-non-fractal transition coefficient, the scale resolution, and the fractal dimension of the movement curves. When compared with experimental data depicting the temporal evolution of the plasma parameters determined through the Langmuir probe method, the model satisfactorily reproduces the experimental traces. In the compact form of the model, we were able to define some clear associations between fractal model variables and specific plasma parameters. From the theoretical fit, we determined a range of values for the fractalization degree which describes the laser-produced plasmas in the ns ablation regime, while more efforts are required to elucidate some features associated with femtosecond laser ablation (e.g. evolution of the oscillation period with the target atomic mass).

Acknowledgements

This work has been partially supported by the Agence Nationale de la Recherche through the LABEX CEMPI (ANR-11-LABX-0007), as well as by the Ministry of Higher Education and Research, Hauts de France Council and European Regional Development Fund (ERDF) through the Contrat de Projets Etat-Region (CPER Photonics4Society). S.A.I. thanks the Institut Français de Bucharest for a BGF cotutelle PhD grant.

Author details

Petru-Edward Nica[1], Stefan Andrei Irimiciuc[2,3], Maricel Agop[1], Silviu Gurlui[2], Michael Ziskind[3] and Cristian Focsa[3]*

*Address all correspondence to: cristian.focsa@univ-lille1.fr

1 Department of Physics, Gheorghe Asachi Technical University, Iasi, Romania

2 Faculty of Physics, "Alexandru Ioan Cuza" University of Iasi, Iasi, Romania

3 Université de Lille, CNRS, UMR 8523, PhLAM—Physique des Lasers Atomes et Molécules, CERLA— Centre d'Etudes et de Recherches Lasers et Applications, Lille, France

References

[1] Eason R, editor. Pulsed Laser Deposition of Thin Films: Applications-Led Growth of Functional Materials. New Jersey: Wiley; 2011

[2] Miotello A, Ossi P, editors. Laser-Surface Interactions for New Materials Production: Tailoring Structure and Properties. New York: Springer; 2010

[3] Gerhard C, Wieneke S, Viöl W, editors. Laser Ablation: Fundamentals, Methods and Applications. New York: Nova Science Publishers; 2015

[4] Russo RE, Mao X, Gonzalez JJ, Zorba V, Yoo J. Laser ablation in analytical chemistry. Analytical Chemistry. 2013;**85**:6162-6177

[5] Cremers D, Radziemski L, editors. Handbook of Laser-Induced Breakdown Spectroscopy. Chichester: Wiley; 2006

[6] Phipps CR, editor. Laser Ablation and Its Applications. New York: Springer; 2007

[7] Rethfeld B, Sokolowski-Tinten K, von der Linde D, Anisimov SI. Timescales in the response of materials to femtosecond laser excitation. Applied Physics A: Materials Science & Processing. 2004;**79**:767-769

[8] Kelly R, Miotello A. On the role of thermal processes in sputtering and composition changes due to ions or laser pulses. Nuclear Instruments and Methods in Physics Research Section B. 1998;**141**:49-60

[9] Peterlongo A, Miotello A, Kelly R. Laser-pulse sputtering of aluminum: Vaporization, boiling, superheating, and gas-dynamic effects. Physical Review E. 1994;**50**: 4716-4727

[10] Shirk MD, Molian PA. A review of ultrashort pulsed laser ablation of materials. Journal of Laser Applications. 1998;**10**:18-28

[11] Leitz KH, Redlingshöfer B, Reg Y, Otto A, Schmidt M. Metal ablation with short and ultrashort laser pulses. Physics Procedia. 2011;**12**:230-238

[12] Bulgakova NM, Stoian R, Rosenfeld A, Hertel IV, Marine W, Campbell EEB. A general continuum approach to describe fast electronic transport in pulsed laser irradiated materials: The problem of Coulomb explosion. Applied Physics A: Materials Science & Processing. 2005;**81**:345-356

[13] Harilal SS, Freeman JR, Diwakar PK, Hassanein A. Femtosecond Laser Ablation: Fundamentals and Applications. In: Musazzi S, Perini U, editors. Laser-Induced Breakdown Spectroscopy Theory and Applications. New York: Springer; 2014. p. 143-166

[14] Geohegan DB, Puretzky AA. Dynamics of laser ablation plume penetration through low pressure background gases. Applied Physics Letters. 1995;**67**:197-199

[15] Geohegan DB, Puretzky AA. Laser ablation plume thermalization dynamics in background gases: Combined imaging, optical absorption and emission spectroscopy, and ion probe measurements. Applied Surface Science. 1996;**96–98**:131-138

[16] Wood RF, Chen KR, Leboeuf JN, Puretzky AA, Geohegan DB. Dynamics of plume propagation and splitting during pulsed-laser ablation. Physical Review Letters. 1997;**79**:1571-1574

[17] Wood RF, Leboeuf JN, Geohegan DB, Puretzky AA, Chen KR. Dynamics of plume propagation and splitting during pulsed-laser ablation of Si in He and Ar. Physical Review B. 1998;**58**:1533-1543

[18] Harilal SS, Issac RC, Bindhu CV, Nampoori VPN, Vallabhan CPG. Temporal and spatial evolution of C_2 in laser induced plasma from graphite target. Journal of Applied Physics. 1996;**80**:3561-3565

[19] Harilal SS, Issac RC, Bindhu CV, Nampoori VPN, Vallabhan CPG. Emission characteristics and dynamics of C_2 from laser produced graphite plasma. Journal of Applied Physics. 1997;**81**:3637-3643

[20] Harilal SS, Bindhu CV, Tillack MS, Najmabadi F, Gaeris AC. Plume splitting and sharpening in laser-produced aluminium plasma. Journal of Physics D: Applied Physics. 2002;**35**:2935-2938

[21] Harilal SS, Bindhu CV, Tillack MS, Najmabadi F, Gaeris AC. Internal structure and expansion dynamics of laser ablation plumes into ambient gases. Journal of Applied Physics. 2003;**93**:2380-2388

[22] Diwakar PK, Harilal SS, Hassanein A, Phillips MC. Expansion dynamics of ultrafast laser produced plasmas in the presence of ambient argon. Journal of Applied Physics. 2014;**116**:133301

[23] Bulgakov AV, Bulgakova NM. Gas-dynamic effects of the interaction between a pulsed laser ablation plume and the ambient gas: Analogy with an underexpanded jet. Journal of Physics D: Applied Physics. 1998;**31**:693-703

[24] Bulgakova NM, Panchenko AN, Zhukov VP, Kudryashov SI, Pereira A, Marine W, Mocek T, Bulgakov AV. Impacts of ambient and ablation plasmas on short- and ultrashort-pulse laser processing of surfaces. Micromachines. 2014;**5**:1344-1372

[25] Harilal SS, Tillack MS, O'Shay B, Bindhu CV, Najmabadi F. Confinement and dynamics of laser-produced plasma expanding across a transverse magnetic field. Physical Review E. 2004;**69**:026413

[26] Anoop KK, Harilal SS, Philip R, Bruzzese R, Amoruso S. Laser fluence dependence on emission dynamics of ultrafast laser induced copper plasma. Journal of Applied Physics. 2016;**120**:185901

[27] Anoop KK, Polek MP, Bruzzese R, Amoruso S, Harilal SS. Multidiagnostic analysis of ion dynamics in ultrafast laser ablation of metals over a large fluence range. Journal of Applied Physics. 2015;**117**:083108

[28] Anoop KK, Ni X, Wang X, Amoruso S, Bruzzese R. Fast ion generation in femtosecond laser ablation of a metallic target at moderate laser intensity. Laser Physics. 2014;**24**:105902

[29] Thestrup B, Toftmann B, Schou J, Doggett B, Lunney JG. Ion dynamics in laser ablation plumes from selected metals at 355 nm. Applied Surface Science. 2002;**197–198**:175-180

[30] Toftmann B, Schou J, Lunney JG. Dynamics of the plume produced by nanosecond ultraviolet laser ablation of metals. Physical Review B. 2003;**67**:104101

[31] Gonzalo J, Siegel J, Perea A, Puerto D, Resta V, Galvan-Sosa M, Afonso CN. Imaging self-sputtering and backscattering from the substrate during pulsed laser deposition of gold. Physical Review B. 2007;**76**:035435

[32] Schou J. Physical aspects of the pulsed laser deposition technique: The stoichiometric transfer of material from target to film. Applied Surface Science. 2009;**255**:5191-5198

[33] Canulescu S, Papadopoulou E, Anglos D, Lippert T, Montenegro MJ, Georgiou S, Döbeli M, Wokaun A. Nanosecond and femtosecond ablation of $La_{0.6}Ca_{0.4}CoO_3$: A comparison between plume dynamics and composition of the films. Applied Physics A. 2011;**105**: 167-176

[34] Bulgakova NM, Bulgakov AV, Bobrenok OF. Double layer effects in laser-ablation plasma plumes. Physical Review E. 2000;**62**:5624-5634

[35] Cleyssens F, Cheesman A, Henley SJ, Ashfold MNR. Studies of the plume accompanying pulsed ultraviolet laser ablation of zinc oxide. Journal of Applied Physics. 2002;**92**: 6886-6894

[36] Hansen TN, Schou J, Lunney JG. Angle-resolved energy distributions of laser ablated silver ions in vacuum. Applied Physics Letters. 1998;**72**:1829-1831

[37] Amoruso S, Armenante M, Berardi V, Bruzzese R, Velotta R, Wang X. High fluence visibleand ultraviolet laser ablation of metallic targets. Applied Surface Science. 1998; **127-129**:1017-1022

[38] Amoruso S, Bruzzese R, Spinelli N, Velotta R. Characterization of laser-ablation plasmas. Journal of Physics B: Atomic, Molecular and Optical Physics. 1999;**32**:R131-R172

[39] Schou J, Amoruso S, Lunney JG. Plume dynamics. In: Phipps C, editor. Laser Ablation and Its Applications. New York: Springer; 2007. p. 67-95

[40] Doggett B, Lunney JG. Langmuir probe characterization of laser ablation plasmas. Journal of Applied Physics. 2009;**105**:033306

[41] Esposito M, Lippert T, Schneider CW, Wokaun A, Donnelly T, Lunney JG, Tellez H, Vadillo JM, Laserna JJ. Pulsed laser ablation of silver: Ion dynamics in the plasma plume. Journal of Optoelectronics and Advanced Materials. 2010;**12**:677-680

[42] Toftmann B, Doggett B, Budtz-Jorgensen C, Schou J, Lunney JG. Femtosecond ultraviolet laser ablation of silver and comparison with nanosecond ablation. Journal of Applied Physics. 2013;**113**:083304

[43] Chen J, Lunney JG, Lippert T, Ojeda-G-P A, Stender D, Schneider CW, Wokaun A. Langmuir probe measurements and mass spectrometry of plasma plumes generated by laser ablation of $La_{0.4}Ca_{0.6}MnO_3$. Journal of Applied Physics. 2014;**116**:073303

[44] Amoruso S, Wang X, Altucci C, de Lisio C, Armenante M, Bruzzese R, Spinelli N, Velotta R. Double-peak distribution of electron and ion emission profile during femtosecond laser ablation of metals. Applied Surface Science. 2002;**186**:358-363

[45] Amoruso S, Armenante M, Bruzzese R, Spinelli N, Velotta R, Wang X. Emission of prompt electrons during excimer laser ablation of aluminum targets. Applied Physics Letters. 1999;**75**:7-9

[46] Sunil S, Kumar A, Singh RK, Subramanian KP. Measurements of electron temperature and density of multi-component plasma plume formed by laser-blow-off of LiF-C film. Journal of Physics D: Applied Physics. 2008;**41**:085211

[47] Kumar A, Singh RK, Thomas J, Sunil S. Parametric study of expanding plasma plume formed by laser-blow-off of thin film using triple Langmuir probe. Journal of Applied Physics. 2009;**106**:043306

[48] Singh SC, Fallon C, Hayden P, Mujawar M, Yeates P, Costello JT. Ion flux enhancements and oscillations in spatially confined laser produced aluminum plasmas. Physics of Plasmas. 2014;**21**:093113

[49] Hutchinson IH. Principles of Plasma Diagnostics. 2nd revised ed. Cambridge: Cambridge University Press; 2005

[50] Griem HR. Principles of Plasma Spectroscopy. Cambridge: Cambridge University Press; 1997

[51] Kirkwood RK, Moody JD, Kline J, Dewald E, Glenzer S, Divol L, Michel P, Hinkel D, Berger R, Williams E, Milovich J, Yin L, Rose H, MacGowan B, Landen O, Rosen M, Lindl J. A review of laser–plasma interaction physics of indirect-drive fusion. Plasma Physics and Controlled Fusion. 2013;**55**:103001

[52] Gurlui S, Sanduloviciu M, Strat M, Strat G, Mihesan C, Ziskind M, Focsa C. Dynamic space charge structures in high fluence laser ablation plumes. Journal of Optoelectronics and Advanced Materials. 2006;**8**:148-151

[53] Gurlui S, Sanduloviciu M, Mihesan C, Ziskind M, Focsa C. Periodic phenomena in laser-ablation plasma plumes: A self-organization scenario. AIP Conference Proceedings. 2006;**812**:279-282

[54] Focsa C, Ziskind M, Ursu C, Gurlui S, Pagnon D, Pellerin S, Pellerin N, Dudeck M. Laser-$BNSiO_2$ ceramics interaction: Simulation of the energy deposition on dielectric wall surfaces in Hall thrusters. Journal of Optoelectronics and Advanced Materials. 2008;**10**:2380-2385

[55] Gurlui S, Agop M, Nica P, Ziskind M, Focsa C. Experimental and theoretical investigations of a laser-produced aluminum plasma. Physical Review E. 2008;**78**:026405

[56] Ursu C, Gurlui S, Focsa C, Popa G. Space- and time-resolved optical diagnosis for the study of laser ablation plasma dynamics. Nuclear Instruments and Methods in Physics Research Section B. 2009;**267**:446-450

[57] Focsa C, Nemec P, Ziskind M, Ursu C, Gurlui S, Nazabal V. Laser ablation of As_xSe_{100-x} chalcogenide glasses: Plume investigations. Applied Surface Science. 2009;**255**:5307-5311

[58] Nica P, Vizureanu P, Agop M, Gurlui S, Focsa C, Forna N, Ioannou P, Borsos Z. Experimental and theoretical aspects of Aluminum expanding laser plasma. Japanese Journal of Applied Physics. 2009;**48**:066001

[59] Agop M, Nica P, Gurlui S, Focsa C. Fractal hydrodynamic model of high fluence laser ablation plasma expansion. AIP Conference Proceedings. 2010;**1278**:612-622

[60] Nica P, Agop M, Gurlui S, Focsa C. Oscillatory Langmuir probe ion current in laser produced plasma expansion. Europhysics Letters. 2010;**89**:65001

[61] Cimpoesu RH, Pompilian GO, Baciu C, Cimpoesu N, Nejneru C, Agop M, Gurlui S, Focsa C. Pulsed laser deposition of poly(l-Lactide) acid on nitinol substrate. Optoelectronics and Advanced Materials, Rapid Communications. 2010;**4**:2148-2153

[62] Ursu C, Pompilian OG, Gurlui S, Nica P, Agop M, Dudeck M, Focsa C. Al_2O_3 ceramics under high-fluence irradiation: Plasma plume dynamics through space-and time-resolved optical emission spectroscopy. Applied Physics A: Materials Science & Processing. 2010;**101**:153-159

[63] Agop M, Nica PE, Gurlui S, Focsa C, Paun VP, Colotin M. Implications of an extended fractal hydrodynamic model. European Physical Journal D: Atomic, Molecular, Optical and Plasma Physics. 2010;**56**:405-419

[64] Focsa C. Laser ablation transient plasma structures expansion in vacuum. IEEE Transactions on Plasma Sciences. 2011;**39**:Gurlui S, 2820-Gurl2821

[65] Nica P, Agop M, Gurlui S, Bejinariu C, Focsa C. Characterization of aluminum laser produced plasma by target current measurements. Japanese Journal of Applied Physics. 2012;**51**:106102

[66] Balika L, Focsa C, Gurlui S, Pellerin S, Pellerin N, Pagnon D, Dudeck M. Laser induced breakdown spectroscopy in a running Hall effect Thruster for space propulsion. Spectrochimica Acta Part B. 2012;**74–75**:184-189

[67] Pompilian OG, Gurlui S, Nemec P, Nazabal V, Ziskind M, Focsa C. Plasma diagnostics in pulsed laser deposition of GaLaS chalcogenides. Applied Surface Science. 2013;**278**: 352-356

[68] Balika L, Focsa C, Gurlui S, Pellerin S, Pellerin N, Pagnon D, Dudeck M. Laser ablation in a running Hall effect Thruster for space propulsion. Applied Physics A: Materials Science & Processing. 2013;**112**:123-127

[69] Dascalu G, Pompilian G, Chazallon B, Nica V, Caltun O, Gurlui S, Focsa C. Rare earth doped cobalt ferrite thin films deposited by PLD. Applied Physics A: Materials Science & Processing. 2013;**110**:915-922

[70] Dascalu G, Pompilian G, Chazallon B, Caltun O, Gurlui S, Focsa C. Femtosecond pulsed laser deposition of cobalt ferrite thin films. Applied Surface Science. 2013;**278**:38-42

[71] Irimiciuc SA, Mihaila I, Agop M. Experimental and theoretical aspects of a laser produced plasma. Physics of Plasmas. 2014;**21**:093509

[72] Irimiciuc S, Agop M, Nica P, Gurlui S, Mihaileanu D, Toma S, Focsa C. Dispersive effects in laser ablation plasmas. Japanese Journal of Applied Physics. 2014;**53**:116202

[73] Bulai G, Gurlui S, Caltun OF, Focsa C. Pure and rare earth doped cobalt ferrite laser ablation: Space and time resolved optical emission spectroscopy. Digest Journal of Nanomaterials and Biostructures. 2015;**10**:1043-1053

[74] Bulai G, Dumitru I, Pinteala M, Focsa C, Gurlui S. Magnetic nanoparticles generated by laser ablation in liquid. Digest Journal of Nanomaterials and Biostructures. 2016; **11**:283-293

[75] Irimiciuc S, Boidin R, Bulai G, Gurlui S, Nemec P, Nazabal V, Focsa C. Laser ablation of $(GeSe_2)_{100-x}(Sb_2Se_3)_x$ chalcogenide glasses: Influence of the target composition on the plasma plume dynamics. Applied Surface Science. 2017;**418B**:594-600

[76] Irimiciuc SA, Gurlui S, Nica P, Focsa C, Agop MA. Compact non-differential approach for modelling laser ablation plasma dynamics. Journal of Applied Physics. 2017;**121**: 083301

[77] Irimiciuc SA, Gurlui S, Bulai G, Nica P, Agop M, Focsa C. Langmuir probe investigation of transient plasmas generated by femtosecond laser ablation of several metals: Influence of the target physical properties on the plume dynamics. Applied Surface Science. 2017;**417**:108-118

[78] Focsa C, Gurlui S, Nica P, Agop M, Ziskind M. Plume splitting and oscillatory behavior in transient plasmas generated by high-fluence laser ablation in vacuum. Appl. Surf. Sci. 2017;**424P3**:299-309

[79] Nica P, Gurlui S, Osiac M, Agop M, Ziskind M, Focsa C. Investigation of Femtosecond Laser-Produced Plasma from Various Metallic Targets using Langmuir Probe Characteristic. Phys. Plasmas. 2017; in press

[80] Puretzky AA, Geohegan DB, Haufler RE, Hettich RL, Zheng XY, Compton RN. Laser ablation of graphite in different buffer gases. AIP Conference Proceedings. 1993;**288**: 365-374

[81] Harilal SS, Farid N, Freeman JR, Diwakar PK, LaHaye NL, Hassanein A. Background gas collisional effects on expanding fs and ns laser ablation plumes. Applied Physics A: Materials Science & Processing. 2014;**117**:319-326

[82] Ojeda-G-P A, Schneider CW, Döbeli M, Lippert T, Wokaun A. Plasma plume dynamics, rebound, and recoating of the ablation target in pulsed laser deposition. Journal of Applied Physics. 2017;**121**:135306

[83] Krása J, Jungwirth K, Gammino S, Krouský E, Láska L, Lorusso A, Nassisi V, Pfeifer M, Rohlena K, Torrisi L, Ullschmied J, Velyhan A. Partial currents of ion species in an expanding laser-created plasma. Vacuum. 2008;**83**:180-184

[84] Kelly R, Dreyfus RW. On the effect of Knudsen-layer formation on studies of vaporization, sputtering, and desorption. Surface Science. 1988;**198**:263-276

[85] Kabashin AV, Nikitin PI, Marine W, Sentis M. Experimental study of spontaneous electric field generated by a laser plasma. Applied Physics Letters. 1998;**73**:25-27

[86] Kabashin AV, Konov VI, Nikitin PI, Prokhorov AM, Konjević N, Vikor L. Laser plasma generation of currents along a conductive target. Journal of Applied Physics. 1990;**68**: 3140-3146

[87] Kabashin AV, Nikitin PI, Marine W, Sentis M. Electric fields of a laser plasma formed by optical breakdown of air near various targets. Quantum Electronics. 1998;**28**:24-28

[88] Wu J, Li X, Wei W, Jia S, Qiu A. Understanding plume splitting of laser ablated plasma: A view from ion distribution dynamics. Physics of Plasmas. 2013;**20**:113512

[89] Gornushkin IB, Panne U. Radiative models of laser-induced plasma and pump-probe diagnostics relevant to laser-induced breakdown spectroscopy. Spectrochimica Acta B. 2010;**65**:345-359

[90] Elsied AM, Termini NC, Diwakar PK, Hassanein A. Characteristics of ions emission from Ultrashort laser produced plasma. Scientific Reports. 2016;**6**:38256

[91] Weaver I, Martin GW, Graham WG, Morrow T, Lewis CLS. The Langmuir probe as a diagnostic of the electron component within low temperature laser ablated plasma plume. The Review of Scientific Instruments. 1999;**70**:1801-1805

[92] Hansen TN, Schou J, Lunney JG. Langmuir probe study of plasma expansion in pulsed laser ablation. Applied Physics A: Materials Science & Processing. 1999;**69**:S601-S604

[93] Dogar AH, Ilyas B, Ullah S, Nadeem A, Qayyum A. Langmuir probe measurements of Nd-YAG laser-produced copper plasmas. IEEE Transactions on Plasma Sciences. 2011;**39**:897-900

[94] Salle B, Chaleard C, Detalle V, Lacour JL, Mauchien P, Nouvellon C, Semerok A. Laser ablation efficiency of metal samples with UV laser nanosecond pulses. Applied Surface Science. 1999;**138-139**:302-305

[95] Schou J, Toftmann B, Amoruso S. Pulsed laser deposition: From basic processes to film deposition. Proceedings of SPIE. 2005;**5830**:1-10

[96] Olivier M, Němec P, Boudebs G, Boidin R, Focsa C, Nazabal V. Photosensitivity of pulsed laser deposited Ge-Sb-se thin films. Optical Materials Express. 2015;**5**:781-793

[97] Afifi MA, Labib HH, Fadel M. Electrical and thermal properties of chalcogenide glass system $Se_{75}Ge_{25-x}Sb_x$. Applied Physics A: Materials Science & Processing. 1992;**55**:167-169

[98] Merches I, Agop M. Differentiability and Fractality in Dynamics of Physical Systems. Singapore: World Scientific; 2015

[99] Krása J, Lorusso A, Doria D, Belloni F, Nassisi V, Rohlena K. Time-of-flight profile of multiply-charged ion currents produced by a pulse laser. Plasma Physics and Controlled Fusion. 2005;**47**:1339-1349

[100] Doria D, Lorusso A, Belloni F, Nassisi V. Characterization of a nonequilibrium XeCl laser-plasma by a movable Faraday cup. The Review of Scientific Instruments. 2004;**75**:387

[101] Kelly R, Miotello A. Comments on explosive mechanisms of laser sputtering. Applied Surface Science. 1996;**96–98**:205-215

[102] Anisimov SI, Luk'yanchuk BS. Selected problems of laser ablation theory. Physics-Uspekhi. 2002;**45**:293-324

[103] Murakami M, Kang YG, Nishihara K, Fujioka S, Nishimura H. Ion energy spectrum of expanding laser-plasma with limited mass. Physics of Plasmas. 2005;**12**:62706